



Modeling E. coli fate and transport in and around a cattle pond

- 3 Alexandr Yakirevich^{1,5}, Alisa Coffin², James Widmer³, Oliva Pisani², Robert Hill¹, Yakov Pachepsky⁴
- ⁴ Department of Environmental Science and Technology, University of Maryland, College Park, MD, 21742, USA
- 5 ²USDA-ARS, Southeast Watershed Research Laboratory, Tifton, GA. 31793, USA
- 6 ³Department of Food Science AND Technology, University of Georgia, Athens, 30602, GA, USA
- 7 ⁴USDA-ARS Environmental Microbial and Food Safety Laboratory, Beltsville, MD, 20705, USA
- 8 ⁵Zuckerberg Institute for Water Research, J. Blaustein Institutes for Desert Research, Ben Gurion University of the Negev,
- 9 Sede Boker Campus, 8499000, Israel
- 10 Correspondence to: Yakov Pacjepsky (yakov.pachepsky@usda.gov)
- 11 Abstract Contamination of surface water is a concern for public health. Lands used for animal production are sources of fecal
- 12 microorganisms that can reach water bodies, impact their quality, and adversely affect their potential uses. Understanding the
- 13 mechanisms of microbial transport through surface/subsurface flow is imperative to predict surface water contamination and
- 14 to assign management strategies for enhanced water quality. The aim of this work to develop and test a mechanistic numerical
- 15 model to simulate watershed-scale surface/subsurface water flow, bacteria release from cow manure, and their fate, as well as
- 16 transport to a cattle pond. The integrated surface-subsurface hydrological platform HydroGeoSphere (HGS) was the basis for
- 17 the site-specific model. The pond and its environs were monitored for 15 months for E. coli concentrations, which remained
- 18 relatively high throughout the study The model was applied to simulate Escherichia coli (E. coli) bacteria transport in a grassed
- 19 drainage basin grazed by a permanent herd of approximately 50 cattle. Most model parameter values were adopted from the
- 20 literature. The model explicitly accounted for cow excretion to the pond as a source of microbial contamination. The latter was
- 21 estimated from the time spent by cows in the pond, which in turn was estimated from imagery obtained with eight trail cameras
- 22 installed to cover the pond surface. Images were obtained every 15 min. Simulations for two years showed that the non-
- 23 calibrated model replicated spatiotemporal patterns and peak E. coli concentration reasonably well. The E. coli cumulative
- 24 flux loaded by cattle excretion directly to the pond was around two orders of magnitude greater than that with the surface flow.
- 25 The results of this work indicate the opportunity and show the approach to obtaining a moderately accurate forecast of microbes
- 26 in cattle ponds using only readily available data.

1. Introduction

- 29 Lands used for animal production, such as cow pastures, are sources of fecal microorganisms that can reach water
- 30 bodies, impact their quality, and adversely affect their potential uses. Water runoff during and after rainfall events is an
- 31 essential factor causing microbial transport from animal waste on pastures to water sources used for irrigation and recreation.
- 32 Public health concerns the fate and transport of pathogenic microorganisms and organisms used as indicators of microbial
- 33 pollution, such as *Escherichia coli* (*E. coli*).
- 34 Mechanistic mathematical modeling has provided essential tools for predicting surface water quality and assessing various
- 35 sources causing environmental contamination. Models represented by a compartmental setup use the mass balance, empirical,
- and semi-empirical equations (Cho et al., 2016; Bradford et al.; De Brauwere et al., 2014; van der Meulen et al., 2024). The





mechanistic models are based on the mathematical description of the momentum and mass balance equations. They account for the physicochemical and biological processes via constitutive relations or sub-models and various sources and sinks internally or through boundary conditions. One of the most popular models of this type is the Soil and Water Assessment Tool (SWAT), which has often been used to simulate the fate and transport of *E. coli* in streams (Sowah et al., 2020; Kondo et al., 2021; Iqbal et al., 2019). Both point and non-point microbial pollution have been simulated. For example, Kuang et al. (2024) used the SWAT model to evaluate *E. coli* concentrations in surface water from domestic sewage and manure in China's Three Gorges Reservoir region. Such models often simulate fecal contamination in rivers, estuaries, and coastal areas (Gao et al. 2015; Wolska et al. 2022). Microbial transport has commonly been approximated as a one-dimensional process. Much less work has been done to simulate 3D flow and transport in environmental settings. Currle et al. (2024) gave an example and developed a model for simulating reactive microbial transport in river-groundwater systems. The model was implemented in the integrated surface-subsurface hydrological platform HydroGeoSphere (HGS) (Therrien et al., 2010). The authors produced a synthetic example emphasizing reactive microbial transport in riverbank filtration settings, aiming to quantify microbial water quality in the aquifer with the pumping wells, which is crucial to improve drinking water management. The HGS software can be applied to various water bodies, including ponds.

Ponds are important sources of agricultural water in rural environments. From 2.6 to 9 million ponds are used for irrigation, recreation, providing water to the livestock, and postharvest processing in the United States (Renwick et al., 2006). Little attention has been paid to modeling microbial water quality in agricultural ponds. Vazquez et al. (2021) developed a mechanistic, runoff-driven bacterial transport model to simulate peak bacterial concentration events for two highly variable irrigation ponds in West Central Florida. The authors assumed that surface runoff driven by rainfall events is the primary mechanism driving microbial contamination in these ponds. The calibrated model predicted *E. coli* peak events relatively well, but did not consider the spatial distribution of pathogens in and around the ponds.

The Georgia Coastal plain, USA, has more than 13,000 farm ponds with typical surface area from one to four hectares (Yao et a, 2024). Many of them are used as cattle ponds, given that the average high summer temperature is around 32 °C. It is common for agricultural producers to impound water by constructing earthen dams across small streams, thereby capturing and storing surface water. Additional water is often pumped from deeper aquifers to supplement the water supply (Albright et al., accepted). These ponds tend to be relatively small (~2 ha) and shallow (<3 m) and may be used for more than one purpose, including irrigation, recreation, aquaculture, and a source of water for livestock, or "cattle ponds." Cattle ponds are farm ponds used by cattle and other livestock animals, providing a perennial supply of available water for drinking and cooling on hot days. Animals stocked in pastures are typically given free access to cattle ponds within the enclosed areas to wander and stay at will. An essential feature of cattle ponds is the direct input of organic matter and enteric microorganisms into the aquatic system when the animals eliminate waste. The microbiological quality of water is an essential issue because these waterbodies are used as a source of drinking water for animals and crop irrigation. This raises concerns regarding microbial contamination of water that may be used for consumption, either by animals or as irrigation inputs. However, to our knowledge, the microbial



72

73

74

75

76

77 78

79

80

81



quality of water in cattle ponds and the factors that influence it are poorly understood, so the scope of the problem is not well known.

The farmers typically lack the resources to monitor their ponds. That limits opportunities for model calibration. Therefore, it may be beneficial to apply modeling and to determine the accuracy of simulating the microbial quality of water that can be achieved without model calibration.

The objectives of this work were to (a) carry out spatiotemporal monitoring of the *E. coli* concentrations in a typical farm pond in Georgia where cattle grazed on the surrounding land had uninterrupted access to water to drink and cool off; (b) monitor and quantify the presence of cattle in the pond, and (c) develop an *E. coli* fate and transport hydrologic model that would include transport of manure borne *E. coli* to the pond, direct deposition of animal waste to the pond, and mixing within the pond.

2. Materials and Methods

2.1. Study area and environment

- 82 The study area is a small watershed (area ~0.45 km²) with a pond within a larger, fenced pasture, located on a privately owned
- 83 crop-livestock integrated farm in the southern Coastal Plain of Georgia, USA (Figure 1a). The farm is referred to as the Sumner
- 84 Cooperator Farm (SCF). Currently, the area is used for cow grazing. The climate is humid subtropical, with a mean annual
- 85 temperature of 18.8 °C and mean annual precipitation of 1174 mm.
- 86 The land surface's Digital Elevation Model of 1 m resolution was downloaded from the Open Topography portal
- 87 (https://portal.opentopography.org/). The altitude of the land surface varies from 101.8 to 119.7 m (Figure 1b).





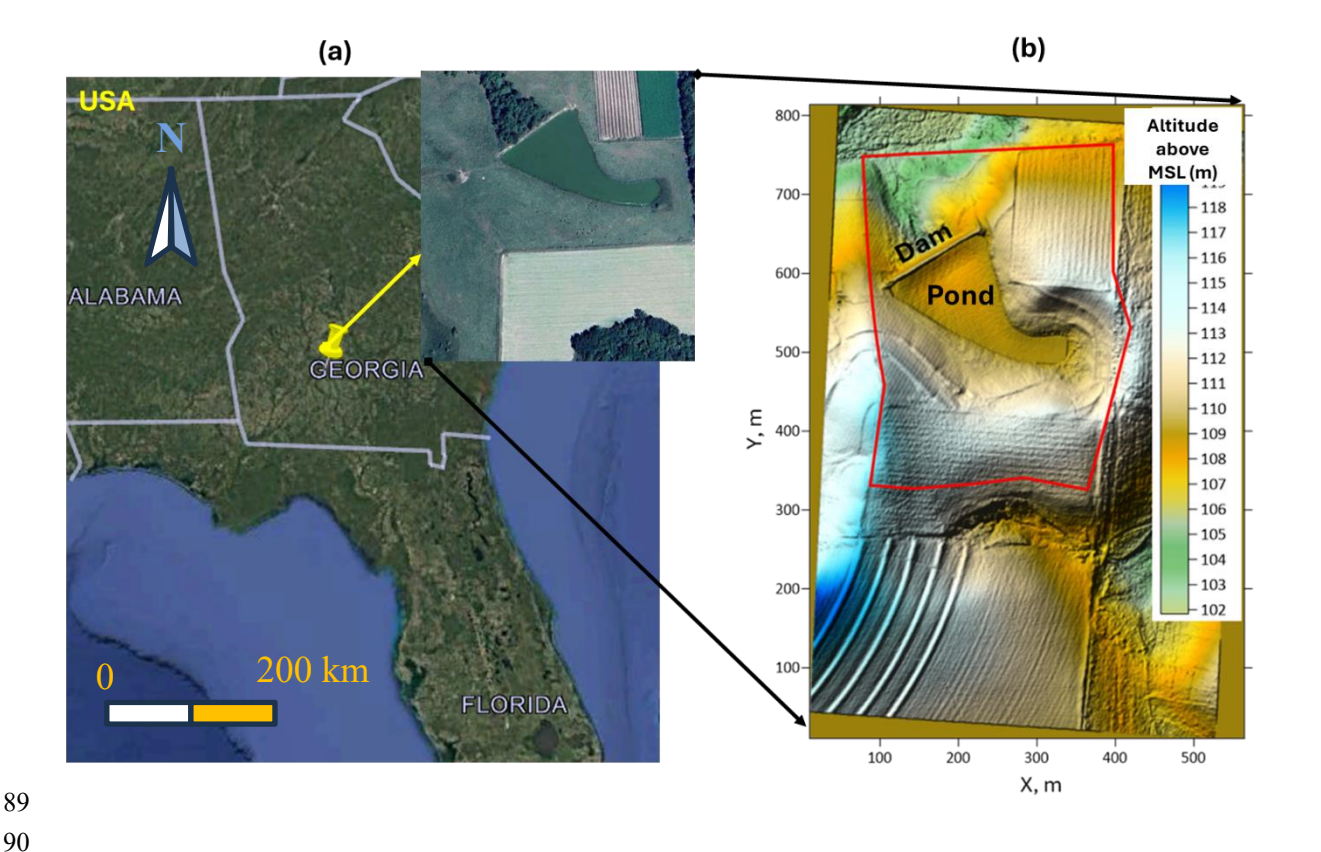


Figure 1. Location from Google Earth(© Google Earth) images (a) and land topography of the study area (b). The red line represents the boundary of the simulation domain,

Soil cover at the site consists of a loamy sand (average of 85% sand, 9% silt, and 7% clay) to depths of 60-80 cm, underlain by sandy clay loam (average of 62% sand, 8% silt, and 30% clay) containing plinthite, a low permeability layer of hard iron-rich soil restricting hydraulic connectivity between surface and groundwater (Blume et al., 1987). The latter soil was used to build the bottom of the pond and the dam.

Weather conditions were monitored by the USDA-ARS Southeast Watershed Research Laboratory (SEWRL) at the site to measure air temperature and humidity, wind speed, solar radiation, and soil and water temperature. Data were collected from a climate station located at the SCF noted as "Rain Gage 80" in the SEWRL public data website (https://radio.tiftonars.org/rg80.htm). Specifications for instrumentation follow the configurations for the Little River Experimental Watershed climate stations described in Bosch et al. (2007).

2.2 Quantifying pond use and bacterial concentrations in cattle manure





Cattle use of the pond and the pasture area draining into the pond was evaluated using automated trail cameras. Eight cameras were fixed to solid structures (e.g., fence posts, trees) and their fields of view (FOVs) captured overlapping images of the pond at regular intervals. Three comparable camera models were used for the study, including 3 Bushnell 24MP Prime Low Glow (Model 119932C), 3 CamPark, and 2 Coleman (Model CHD400W) cameras. Cattle in the pond were imaged from July 2022 to December 2023. Secure digital (SD) removable media cards were used to record the imagery and were replaced every 6 to 10 weeks for the duration of the study. Imagery was downloaded and stored on a file server for subsequent analysis. The imagery was visually assessed for pond use by cattle by a single observer for all days. Images were reviewed from each camera, and the number of cows in the pond was counted in each image. Tallied viewpoint counts were summed according to the model finite element mesh (FEM) nodes segmentation of the shoreline described below, multiplied by the time interval of the camera setting (5 to 30 minutes), and divided by 1440 minutes per day. The resulting values were summed for each shoreline segment to produce a daily value of "cow days" (Cex). To evaluate the accuracy of the visual assessment, two additional independent observers conducted validation counts of a sample of the imagery following the same protocol, and agreement among the three observers (OBS1, OBS2, and OBS3) was evaluated (Table S1).

Between February and May 2023, 18 fresh cow manure samples were collected from the area around the pond. Samples were collected into 50-mL conical tubes using a sterilized tongue depressor and were then placed on ice for storage and transport to the laboratory. Laboratory processing of manure samples occurred within 24 hours of sample collection. Briefly, 2g of manure was blended with 200 mL of sterile, deionized water for 2 min on the highest setting. Mixed samples were then allowed to settle for 15 minutes before aliquots were used to prepare serial dilutions of the manure mixture. Diluted manure solutions were processed in duplicate using the Colilert method (IDEXX, Westbrook, Maine), which produced a most-probable-number (MPN) of *E. coli* in each sample. An MPN was then calculated per mass of manure (MPN *E. coli* kg-1) using information from a dry weight analysis of the manure.

2.3. Water sampling

Figure 2 shows the locations of the water sampling points for measurements of *E. coli* concentration and of the camera viewpoints for monitoring cattle. For the water sampling points, locations with even numbers (2, 4, 6, 8, 10, 12, 14, 16, not shown) have coordinates the same as as locations with odd numbers (1, 3, 5, 7, 9, 11, 13, and 15), respectively. However, locations with odd numbers were sampled at the pond surface, whereas locations with even numbers were sampled at a depth of 50 cm using a peristaltic pump. Locations 17 to 26 were sampled at the surface near the banks.







Figure 2. Locations of water sampling points (1-26) and cattle monitoring cameras (Viewpoints 1-8). The insert shows an example of an image taken at monitoring viewpoint 2. Orthoimage from July 7, 2022 by USDA-ARS, Southeast Watershed Research Laboratory, Remote Sensing and Mapping Group, Tifton, Georgia, USA. The imagery was collected with a Hasselblad L1d-20C 20mp camera using a DJI Mavic 2 Pro L1P drone, and created using Pix4D Mapper image processing software.

2.4 Mathematical model

Accounting for the complexity of hydrogeological and hydrochemical processes, we choose the HGS (Therrien et al., 2010) as a basis for the model. In HGS, the flow of water is simulated in a fully integrated mode; water derived from rainfall inputs is partitioned into components such as overland and stream flow, evaporation, infiltration, recharge, and subsurface discharge into surface water features such as lakes, streams, and wetlands in a natural, physics-based fashion. It employs a fully coupled



148

149

150 151

152

153 154

156

157

158

163

164

165

166 167



146 numerical approach, allowing the simultaneous solution of both the surface and variably saturated subsurface flow, solute

147 transport, and heat transfer.

The mathematical model of the watershed flow and transport comprises the following components. The Richards equation simulates three-dimensional transient subsurface flow in a variably saturated porous medium (PM domain). The van Genuchten (1980) relations are used to calculate the pressure-saturation relationship and hydraulic conductivity. The two-dimensional depth-averaged diffusive wave equation describes overland water flow (OVL domain). The subsurface and surface flow equations are fully coupled. Evapotranspiration affects surface and subsurface flow domains and is modeled as a combination of transpiration from vegetation and evaporation. Microbial transport is described by 3D and 2D coupled advection-dispersion equations in the subsurface and surface, respectively. We chose the linear Henry isotherm for simulating E. coli sorption. A first-order decay reaction describes the bacteria's die-off. The numerical solution of partial differential equations and the initial

155

2.4.1. Finite element mesh

159 The numerical setup of the simulation domain is shown in Figure 3. The lateral boundary was chosen to cover most of the area 160 where runoff water flows towards the pond. The 2D triangular finite element mesh (FEM) was created using AlgoMesh software (www.hydroalgorithmics.com/software/algomesh) (Figure 3a). It consists of 2882 nodes and 5595 triangular 161

162 elements. The mesh has the highest density of nodes and elements near the pond boundary.

and boundary conditions are done by the control volume finite element approach.

The base of the simulated profile is located at the depth corresponding to an altitude of 100 m. The thickness between the base and soil surface was divided into three layers (U1-U3, Figure 3b), and each layer was split into 2 to 4 sublayers. The floors of the layers U2 and U1 are located at depths of 0.1 and 1.0 below the land surface, respectively, thus mimicking the surface topography. In the model, each sublayer is considered an independent layer defining the height of triangular prisms, which presents the vertical extension of the 2D plane mesh within each layer (Figure 3c).



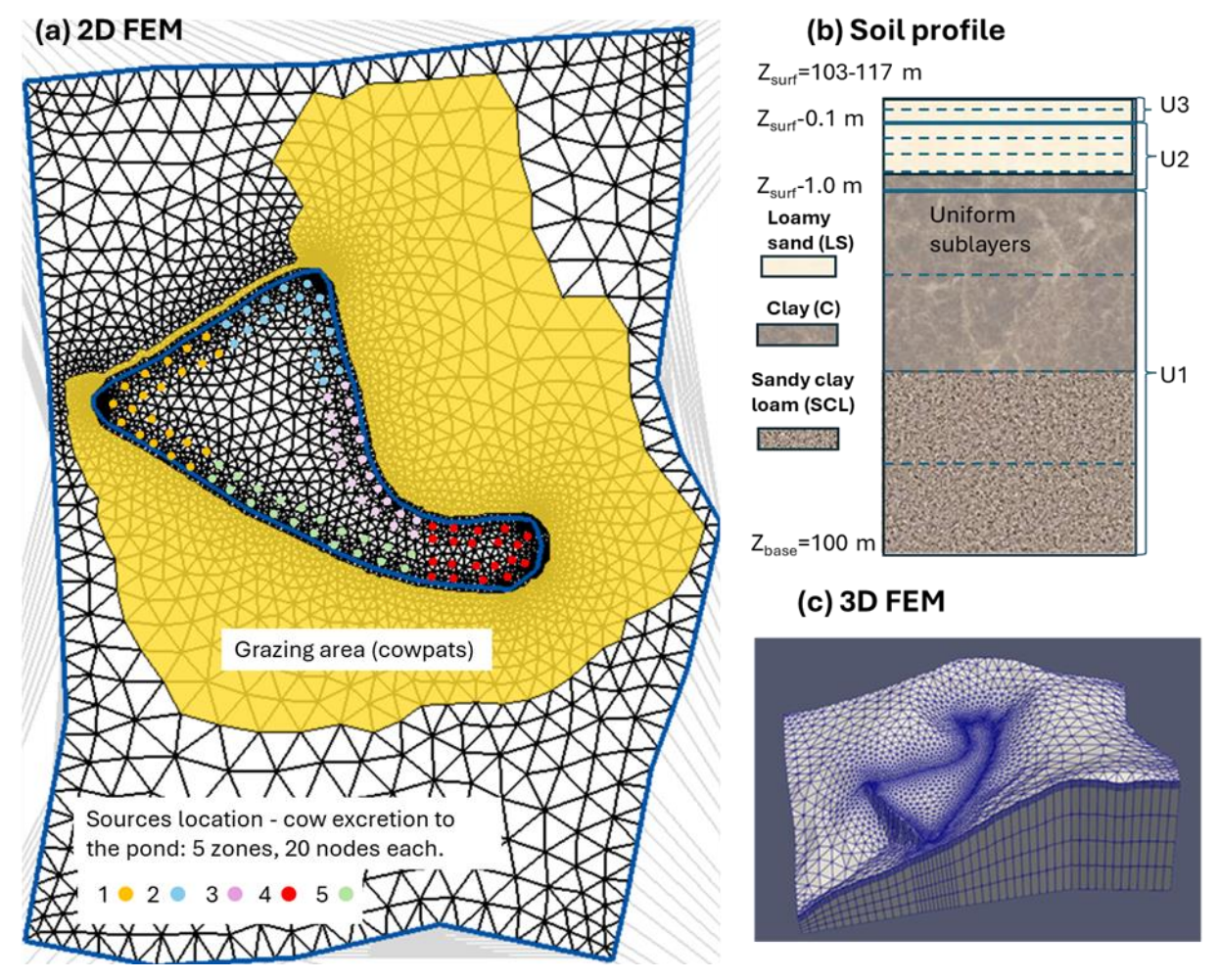


Figure 3. Numerical model setup: (a) The 2D triangular finite element mesh in the simulation domain. Cowpats (a flat, round piece of cow dung) are located in the yellow color area. Colored circles represent the location of sources to simulate cattle excretion in the pond. (b) Schematic representation of numerical mesh layers in the simulated profile. Solid and dashed horizontal lines represent the boundaries between layers and sublayers, respectively. (c) 3D finite element mesh (FEM).

2.4.2. Initial conditions

Initial conditions were obtained by running multi-year simulations. For the subsurface flow, a constant head of -2 m in each node of the finite element mesh was used. For the surface domain, the initial water depth was 10^{-7} m in each node, i.e., the pond was assumed to be empty. These initial conditions were corrected during simulations: 1) For two years, a constant precipitation rate (flux at the soil surface of 0.01 m/day) was simulated to "fill in" the pond with water and establish a steady-state flow regime in the simulation domain; 2) the resulting distribution of heads was taken as a new initial condition and the





model was run with varying precipitation and evapotranspiration for 6 years to establish a quasi-stationary flow regime; 3) Finally, the initial conditions were taken from the results obtained at the end of the simulations.

Initially, the prescribed concentration of bacteria was equal to 0 everywhere in the domain. Then, during multi-year simulations, a concentration distribution was developed in the simulation domain, exhibiting cyclic behavior with time, and it was accepted as the initial condition for January 1, 2022.

2.4.3. Boundary conditions and internal source terms

In the study area, the groundwater level of a regional artesian aquifer was detected at around 70 meters above mean sea level (mamsl) (Watson, 1976), which is 30 m below the bottom (100 m) of the simulated domain. Therefore, the groundwater is not included in simulations. The free drainage boundary condition at the bottom and no flux at the lateral boundaries were prescribed.

At the soil surface, time-variable precipitation rate and evapotranspiration were prescribed. The latter is calculated from the potential evapotranspiration, computed using the Penman-Monteith equation (Monteith, 1981; Danielescu, 2022).

The critical depth boundary condition at the watershed boundary was set to the surface flow domain. The rainfall and evaporation rates are prescribed as volumetric flow fluxes per unit area.

For the bacteria transport, zero-gradient and zero-concentration conditions were set in the subsurface domain along the inflow and outflow lateral boundaries, respectively. The third-type (Cauchy) boundary condition was set at the surface, expressing the balance between bacteria's advective flux at the soil surface and their advective and dispersive fluxes below. The land surface is divided into a grazing area with cowpats and the rest (Figure 3a). Cowpats were assumed to be uniformly distributed over the grazing area. The boundary concentration (and mass flux) equals zero in the area free from cowpats. For the grazing area, a sub-model was developed to calculate the boundary concentration of bacteria. The sub-model simulates the daily evolution of concentration depending on the load of cowpats and the initial concentration of bacteria (see Appendix A for the equations). On each specific day, the fate of bacteria concentration in cowpats that were loaded during that and every previous day was calculated using the Q10 model (Martinez et al., 2013). The latter computes the bacteria's die-off/survival rate depending on weather conditions. The concentrations of released microorganisms are calculated as a function of precipitation according to Bradford and Schijven's (2002) equations for each cowpat's load, accounting for the remaining mass of bacteria during the current day. The resulting boundary concentration is assessed as a sum of those concentrations.

Cattle excretion to the pond was simulated by introducing the internal source terms in the FEM nodes (Figure 3a). The nearshore pond area, where bathing cattle were observed, was divided into five zones. Each zone includes twenty FEM nodes. These nodes do not coincide with the water sampling locations. The source rates were calculated from the number of cattle and the time they spent in the pond (Section 3.1). The time-variable boundary conditions and source/sink terms were prescribed on a daily scale.



218

223224



213 2.5. Model parameters

- We adopted the values of model parameters from different sources or estimated based on existing experimental data or during
- simulations. Tables 1 and 2 present parameter values used in the simulations.

Table 1. The model parameter values for the subsurface domain.

Parameter	Soil			Source
	Loamy sand	Sandy clay	Clay	
		loam		
Hydraulic conductivity K_s , m d ⁻¹	1.2(1.28)	0.35(0.36)	0.0001-0.01	Using Rosetta & PSD ¹
Porosity qs	0.39(0.36)	0.45	0.48 (0.46)	Using Rosetta & PSD
Residual water content q _r	0.049(0.046)	0.08	0.067(0.098)	Using Rosetta & PSD
van Genuchten α, m ⁻¹	3.12(3.6)	2.35(2.29)	2.0 (1.5)	Using Rosetta & PSD
van Genuchten β	1.48(2.02)	1.36(1.35)	1.41(1.25)	Using Rosetta & PSD
Longitudinal dispersivity a_L , m	12.5			Assessed by trial-and-error
Transverse dispersivity a_T , m	2.5			Assigned a_T =0.2 a_L
<i>E. coli</i> distribution coeff. k_D , L kg ⁻¹	14.5			Mankin et al. (2007)
E. coli die-off rate, $k_{s,m,2}(20)$, d ⁻¹	0.042(cowpats), 0.111(soil)			Martinez et.al. (2013)
Parameter $Q_{10,m}$	1.48(cowpats), 1.65(soil),			Park et. al. (2016)

217 ¹PSD – particle size distribution

The geology of the subsurface is not well known. The following composition of soil layers was accepted, based on available information: loamy sand to a depth of 0.5 m, below which a clay layer of variable thickness extends down to the upper half of layer U1 (Figure 3b). The lower half of U1 is presented by sandy clay loam. The pond bottom (to 0.5 m depth) and the dam are built from clay.

Table 2. The model parameter values for the surface and evapotranspiration domains.

Parameter	Value	Source
Manning X friction factor S_{fx} , m ^{-1/3} s	0.3 (grassland), 0.03 (pond)	HGS Introductory Manual
Manning Y friction factor S_{fy} , m ^{-1/3} s	0.3 (grassland), 0.03 (pond)	HGS Introductory Manual
Rill storage height, m	0.05 (grassland), 0.01 (pond)	HGS Introductory Manual
Coupling length l_{etch} , m	0.01	HGS Introductory Manual
Longitudinal dispersivity a_L , m	5-15	Assessed by trial-and-error
Transverse dispersivity, a_T m	1-3	Assigned a_T =0.2 a_L
E. coli die off rate, $k_{s,m,2}(20)$, d^{-1}	0.056	Blaustein et. al (2013)





Parameter $Q_{10,m}$	1.415	Blaustein et. al (2013)
Evaporation depth, m	0.3	HGS Introductory Manual
Root depth, m	1.8	
Leaf area index (LAI)	2.08	HGS Introductory Manual
Transpiration fitting parameters: C1, C2, C3	0.1, 0.05, 2.0	HGS Introductory Manual
Wilting point pressure head, m	-150	HGS Introductory Manual
Field capacity pressure head, m	-3.8	HGS Introductory Manual
Evaporation limiting pressure heads	Min: -1.5, Max: -0.5	HGS Introductory Manual
Canopy storage parameter	0.	HGS Introductory Manual

225226

227

228

229230

231

232

233

234235

236

237

238

E. coli fate and transport simulations were performed for 2022-2023. To progress the numerical convergence and reduce simulation time, we use relative concentrations $C_r = C/C_{max}$, where $C_{max} = 1.4 \cdot 10^{10}$ MPN·m⁻³ is the maximum value of boundary concentration at the soil surface. The value of the longitudinal dispersivity values for the porous media domain was chosen to be 10 m, considering the scale problem (Neuman, 1990). There is no data concerning longitudinal dispersivity for the overland flow domain. Therefore, we tested a few values of this parameter from 5 to 15 m. Longitudinal dispersivity equal to 12.5 m produced a better agreement between simulated and observed concentrations. The transverse dispersivities were 1/5 of the longitudinal ones for porous media and overland flow domains.

The *E. coli* temperature-dependent die-off in manure, soil, and water was simulated. The current version of HGS does not allow the die-off rate in the surface flow domain to be prescribed as a function of temperature. Therefore, this parameter was calculated for each three-month-long season using mean temperature values and used piecewise by restarting simulations for each time interval.

3. Results and discussion

- **3.1.** *E. coli* boundary conditions and internal source terms
- All simulations were carried out using available weather data for a time interval from January 1, 2021, to December 31, 2023.
- Annual precipitation was 1375, 998, and 1167 mm in 2021, 2022, and 2023, respectively. Figure 4 shows rainfall and calculated
- potential evapotranspiration in the study area in 2021-2023.





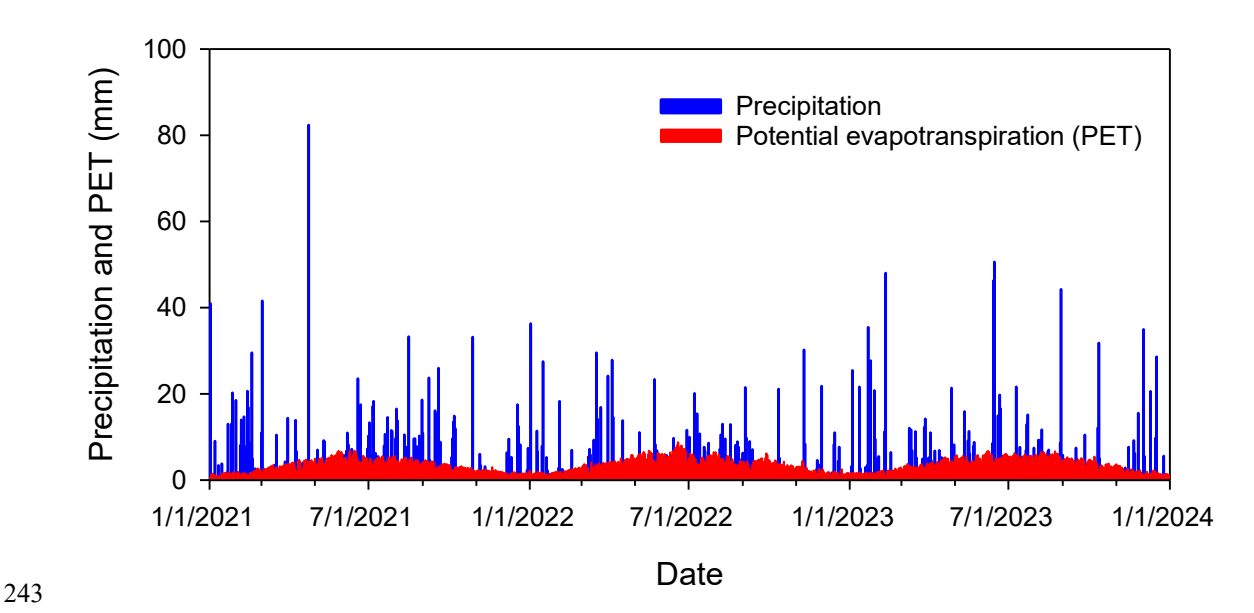


Figure 4. Precipitation and calculated potential evapotranspiration.

The surface Cauchy-type boundary concentration at the grazing area (Figure 3a) was calculated using the equations presented in Appendix A, as described above in section 2.3.3. We assume that 50 cattle (the maximum number of animals that appeared in monitoring camera photos) were grazing in the watershed. The total grassland area of around 60000 m² was estimated based on recent aerial imagery provided in Google Earth (version Pro 7.3). Nennich et al. (2005) estimated the average daily load of manure of 38.6 and 66.3 kg·day⁻¹·cow⁻¹ for dry and lactating cows, respectively. The ratio of urine to feces in dairy cows varies, but on average, slightly less than one-third of manure is urine. Thus, we estimate average daily feces excretion as 0.5*(38.6+66.3)*0.667=35 kg·day⁻¹·cow⁻¹. Monitoring shows that during the day, cows usually graze for at least 12 hours. Therefore, we estimate solid manure load M_0 = kg·day⁻¹·cow⁻¹*12h/24h*50cows/60000m² 0.0146 kg·m⁻². The initial concentration of *E. coli* in fresh cowpats, $m_{i0} = 7.38\cdot10^8$ MPN·kg⁻¹, was calculated as an average in 16 samples collected in 2023. Other parameters in equations A3-A4 were $\alpha_m = 23.375$ h⁻¹, $\beta_m = 1.732$, and E_r =1 (Stoker et al., 2018). No cattle were observed in the field each year from the beginning of December to the end of February. Figure 5 shows the calculated boundary concentrations.





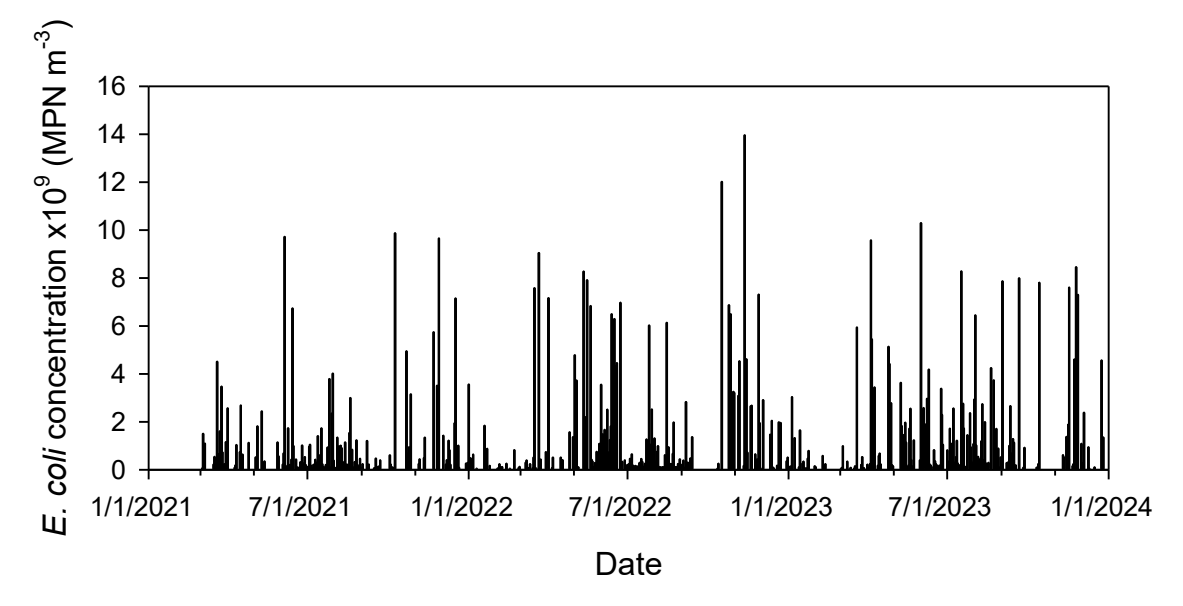


Figure 5. Simulated temporal variation of E. coli surface boundary concentration at the grazing land.

The influx of source terms simulating E. coli load by direct cattle excretion to the pond, as described above, with results shown in Table S1. Validation of the visual assessment of trail camera imagery to derive Cex yielded strong correlations among the three observers (OBS1 v OBS2, n = 64, R^2 = 0.93; OBS1 v OBS3, n = 46, R^2 = 0.90; OBS2 v OBS3, n = 18, R^2 = 0.99). It was assumed that all bacteria were immediately released from manure in the pond. Accounting for the daily cow excretion (as explained above for the surface boundary concentration) and E. coli concentration in cowpats, we calculated the daily source rate for each pond zone (Figure 6) as a portion of the daily manure excretion. The rate for each node is one-tenth of the zone rate. Cattle use monitoring started in July 2022. Therefore, in simulations for the period January-June 2022, where there were no observations, the calculated rates for 2023 were used.





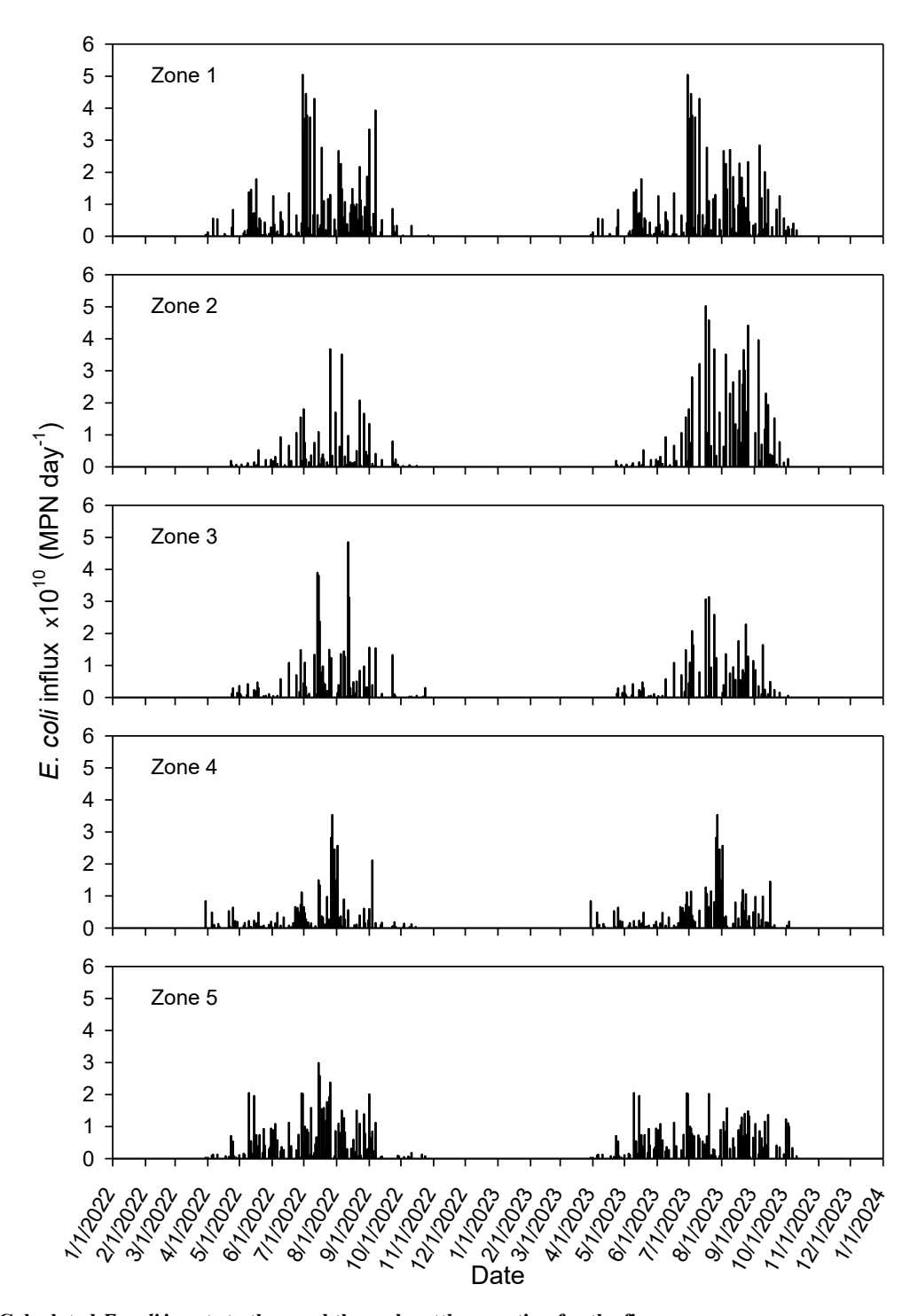


Figure 6. Calculated *E. coli* inputs to the pond through cattle excretion for the five zones.



3.2. Flow simulation results

Water flow simulations were carried out for 2021-2023. The saturated hydraulic conductivity of the clay layer was 0.0002 m·day⁻¹. This value was obtained by trial-and-error fitting to keep the pond from emptying and overflowing during multiannual simulations. The rest of the parameters are presented in Table 1. During periods with high precipitation, perched water was developed above the clay layer (around 0.5 m below the land surface, not shown). Daniels et al. (1978) reported that soil horizons having 10% of platy plinthite will perch water.

Runoff is rarely observed in the area. Simulations show that it usually occurs during and after rain events. The HGS calculates fluid fluxes through the pond boundary. Water fluxes are computed between active nodes (on the boundary of the pond – dark blue dots in Figure 3a) and contributing nodes (just outside the pond boundary). The calculated surface water flux represents simulated runoff to the pond.

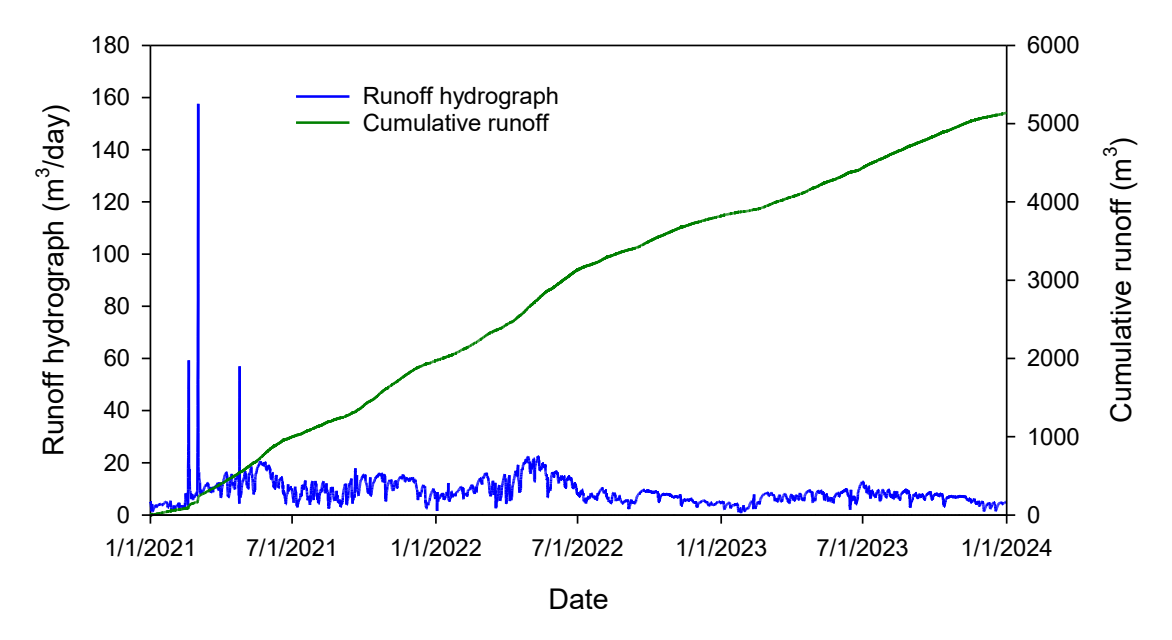


Figure 7. Computed runoff to the pond.

in water volume from 10770 to 16075 m³.

At the beginning of 2021, three significant flow events occurred after intensive 30, 50, and 82 mm rainfalls on February 18, Mar 1-2, and April 24, respectively. During the rest of the time, the average computed surface flow rate to the pond is around 4.4 m³·day⁻¹. The latter is a relatively small value given a 650 m-long pond perimeter.

Simulated changes to pond water volume (m³) and water level (mamsl) were tracked over the study period (Figure 8). The simulated minimal and maximal water levels were 109.03 and 109.37 mamsl. A rise in water level by 0.34 m causes an increase



292293

294

295

296297

298299

300301

302

303

304



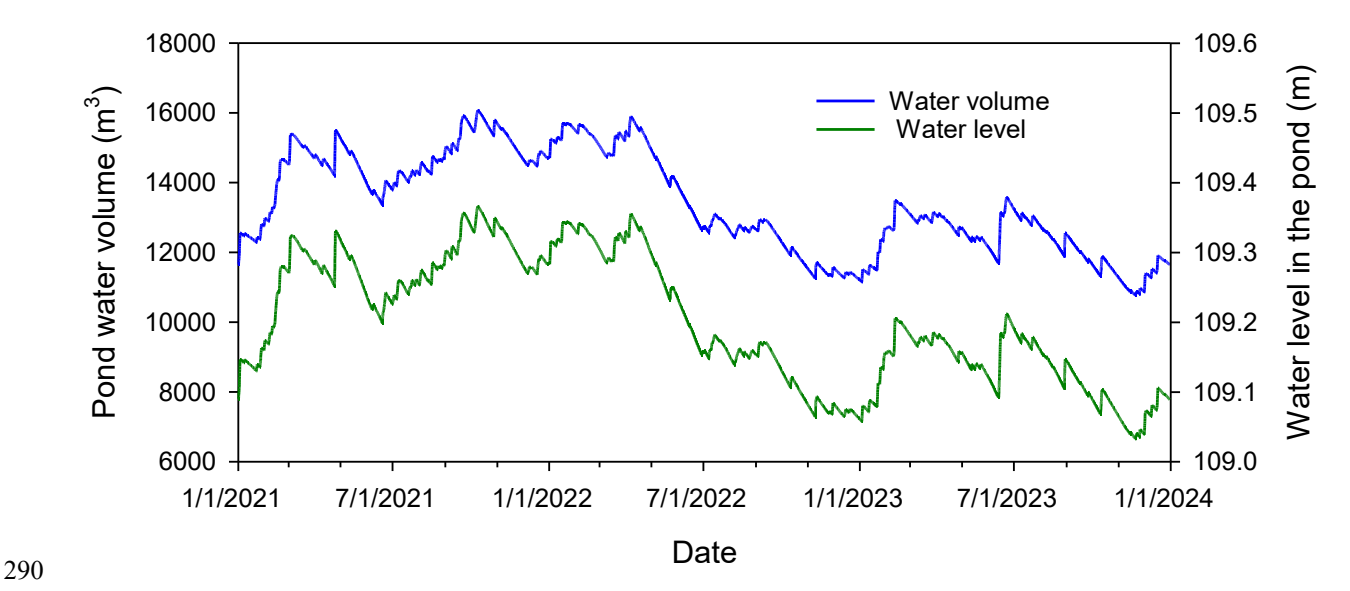


Figure 8. Simulated temporal variation of water volume and level in the pond (above mean sea level).

3.3. Bacteria fate and transport simulations

3.3.1. Results for individual locations

Observed and simulated *E. coli* concentrations in the interior and nearshore pond sampling locations were compared for each sample location (Figures 9 and 10). The non-calibrated model tolerably mimicked *E. coli* concentration patterns and times of peak events in many of the pond's sampling locations. Concentrations increased during summer and decreased during winter months.

For the internal sampling locations 1 to 15, correlation coefficients between the monitored and simulated E. coli concentrations varied between 0.24 and 0.44. An exception was location 7, where the correlation coefficient was -0.01. For the near-shore sampling locations 17 to 26, the correlation coefficient varied between -0.15 and 0.32.



307



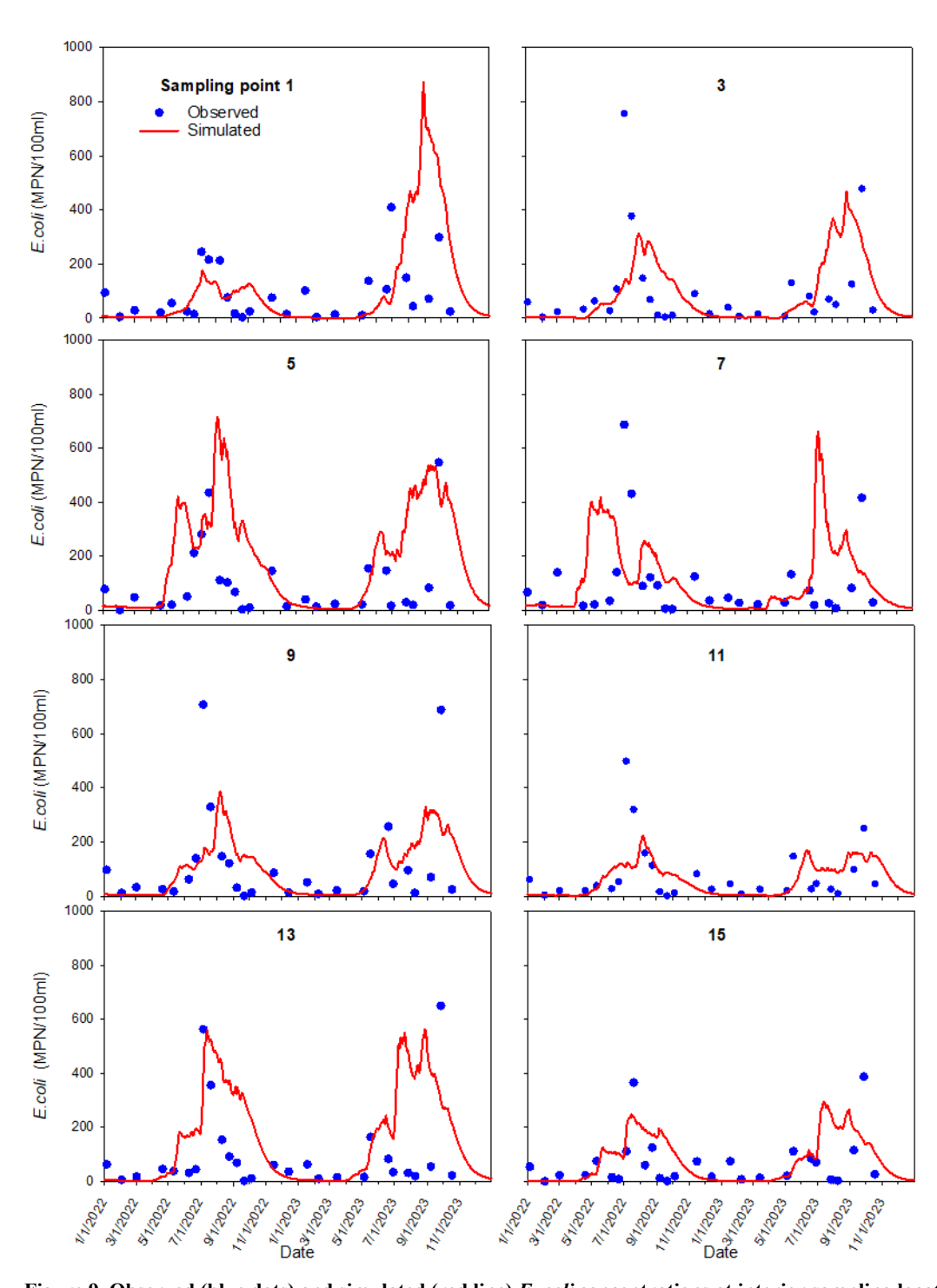


Figure 9. Observed (blue dots) and simulated (red line) E. coli concentrations at interior sampling locations 1-15.





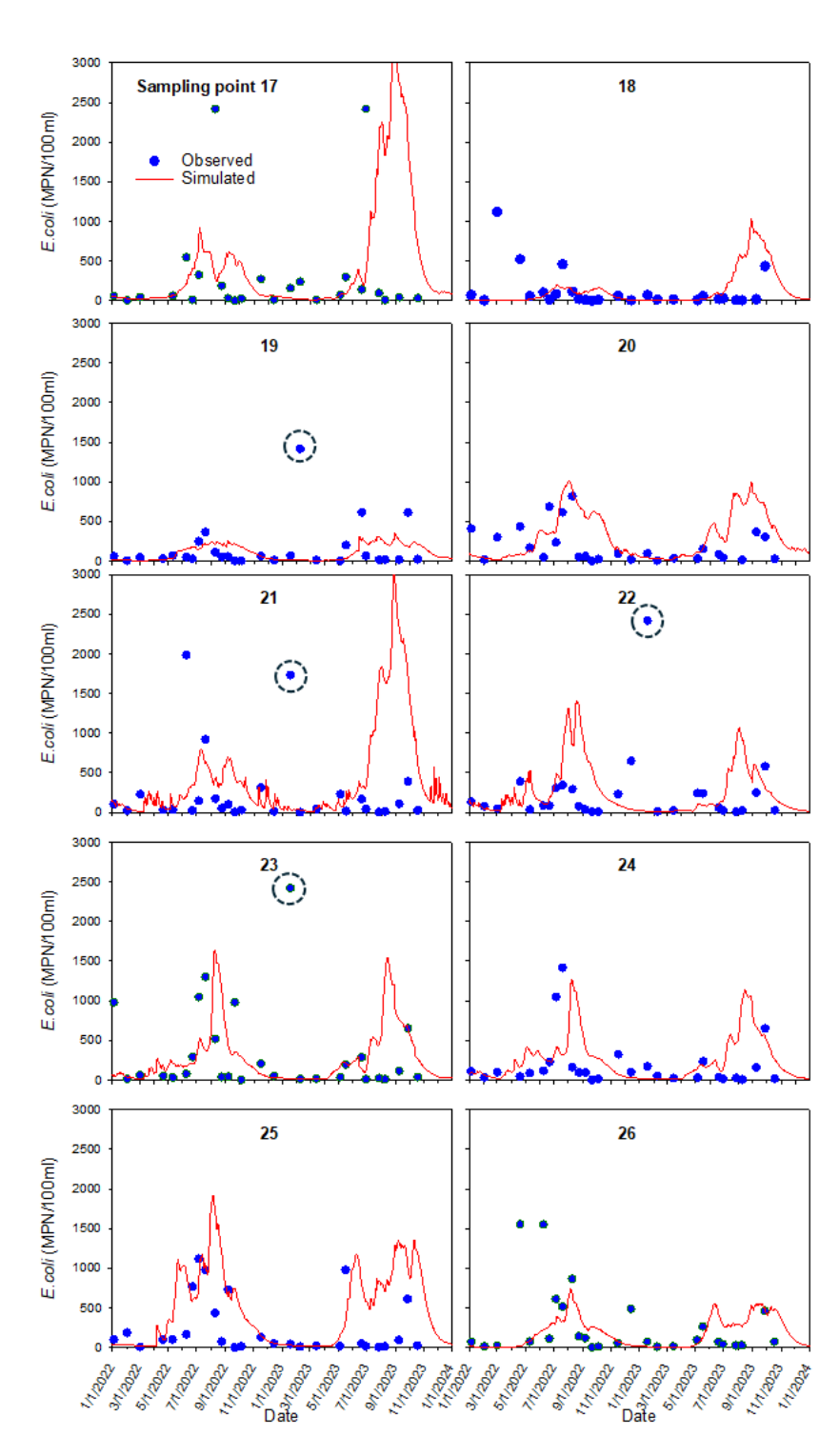






Figure 10. Observed (blue dots) and simulated (red line) *E. coli* concentrations at nearshore sampling locations 17-26. Dashed circles indicate winter increases in concentrations on January 18, 2023.

The observed differences between simulated and measured concentrations in individual sampling locations might originate from the model setup and computational features. The simulated concentration peaks strongly depended on the proximity of the sampling points to the internal source locations, which were constant in time. Cattle frequently moved across the pond in different directions, which affected the concentration distribution. Most assigned locations for the pond's internal source were 10-20 m from the nearest sampling point.

The reproduction of mixing in the pond might be locally unsatisfactory. Figure 11 shows the simulated relative *E. coli* concentration distribution at the surface for different dates. Concentration in the pond source locations rises during summer and dissipates in the winter. Simulations show a low *E. coli* concentration zone in the middle of the pond during the entire simulation period. For example, the model underpredicts peak concentration at sampling location 15 (Figure 9) in summer 2022 and autumn 2023. This indicates that mixing in the pond was stronger than the dispersion mechanism suggests. Lateral transport is often dependent on persistent wind-forced circulation. Henderson et al. (2024) describe wind-forced processes responsible for ponds' vertical mixing or lateral transport. Additional mixing resulting from induced eddies may cause more rapid cross-pond mixing and potentially affect pond ecology and biogeochemistry. At sampling location 23, the increase in concentration could be due to the occasional resuspension of bacteria from the bottom sediments during sampling.



331



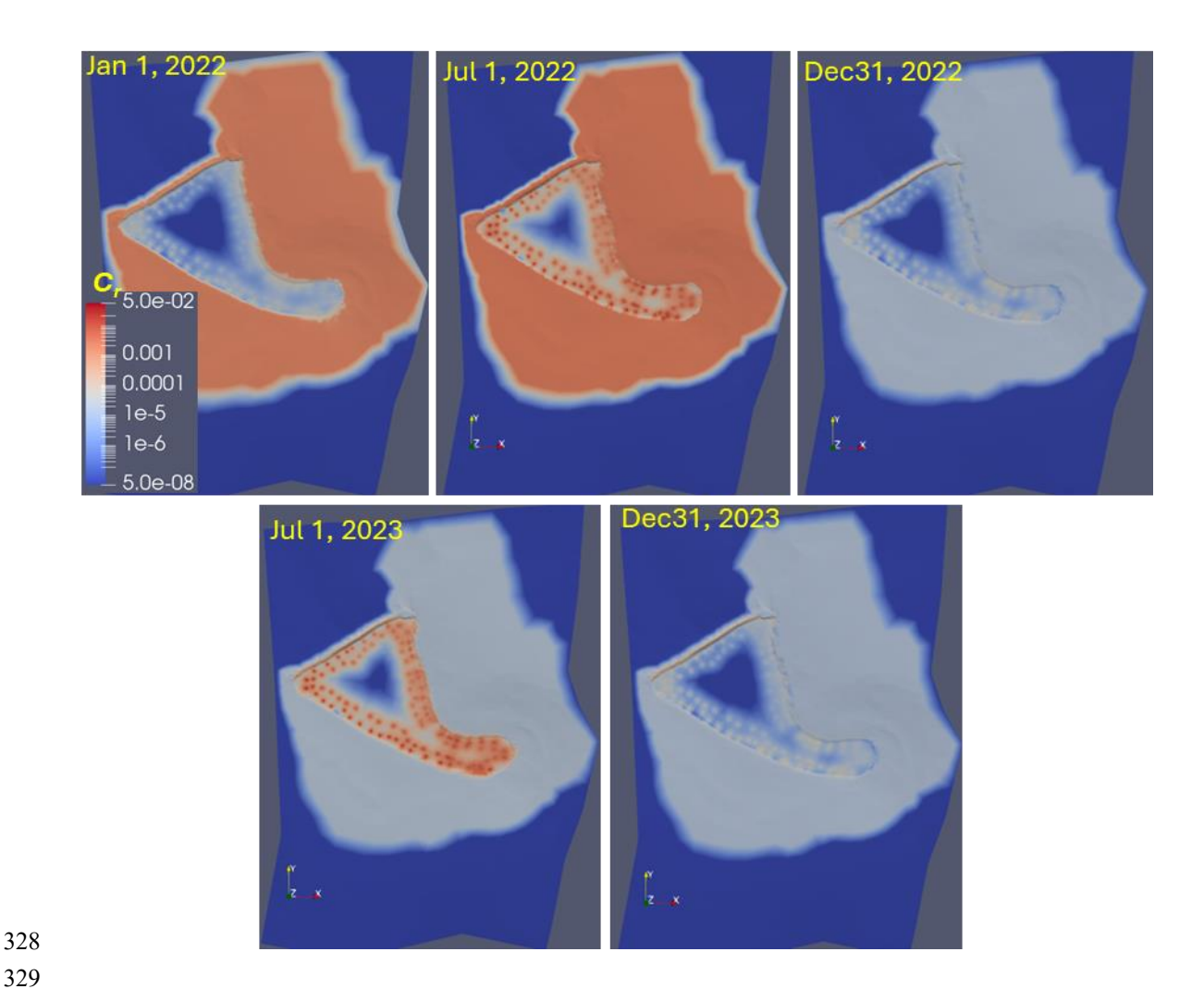


Figure 11. Simulated spatiotemporal distribution of the relative *E. coli* concentration at the surface. $C_r = C/C_{max}$, $C_{max} = 1.4 \ 10^{10}$ MPN·m⁻³, the legend is on a log scale.





More insight could be expected from considering the specifics of *E. coli* survival in waters rich in organic matter and nutrients (Cho et al., 2021). Blaustein et al (2014) analyzed the database on *E. coli* survival in various surface waters. They found that the logarithm of *E. coli* remained approximately constant or even grew for some "shoulder" time after the inactivation experiments in wastewaters with high content of organic matter and nutrients. After the "shoulder" period. The dependence of log C on time changed to a linear decrease. No model has been proposed to estimate the duration of the shoulder period in wastewater so far.

A sudden rise in *E. coli* concentration was observed on January 18, 2023, at sampling locations 19, 21, 22, and 23 (Figure 9, dashed circles). The model does not reproduce this increase. The monitoring camera photos show flocks of birds in the pond near the first three locations 1 to 2 days before the sampling date. At the same time, the model's internal sources on that day were equal to zero since there were no cattle in the pond. We hypothesized that excretion by birds was a reason for elevated *E. coli* concentrations. During the fall and winter, Georgia's inland freshwaters become populated with waterfowl such as ducks, Canada geese, and migratory birds (Balkcom et al., 2025). One duck generates on average 3.8· 10¹⁰ *E. coli* CFU per day (Moriarty et al., 2011), which is similar to the daily *E. coli* output from one cow (4· 10^{\cap10} MPN (g wet feces)⁻¹ day⁻¹ in this work). It appears that the contribution of waterfowl can be very substantial in comparison with cattle contributions (see Figure 5). To our knowledge, the fraction of waterfowl excreta that enters water has not been reported in the literature. Overall, we concur with Vasquez et al. (2021) who emphasized the need to collect more data on the fecal contamination inputs of the ponds.

3.4. Results for the pond as a whole

The HGS computed temporal *E. coli* fluxes entering the pond with surface water. The influxes of *E. coli* to the pond were visualized along with their calculated cumulative numbers over time for both sources of runoff (Figure 12a) and direct excretion (Figure 12b). At the end of simulations, the number of bacteria entering the pond by manure excretion was around 130 times greater than by surface runoff. Simulations show that water was mainly leaving the pond to the subsurface, so concentrations of *E. coli* in the subsurface did not affect water quality in the pond.





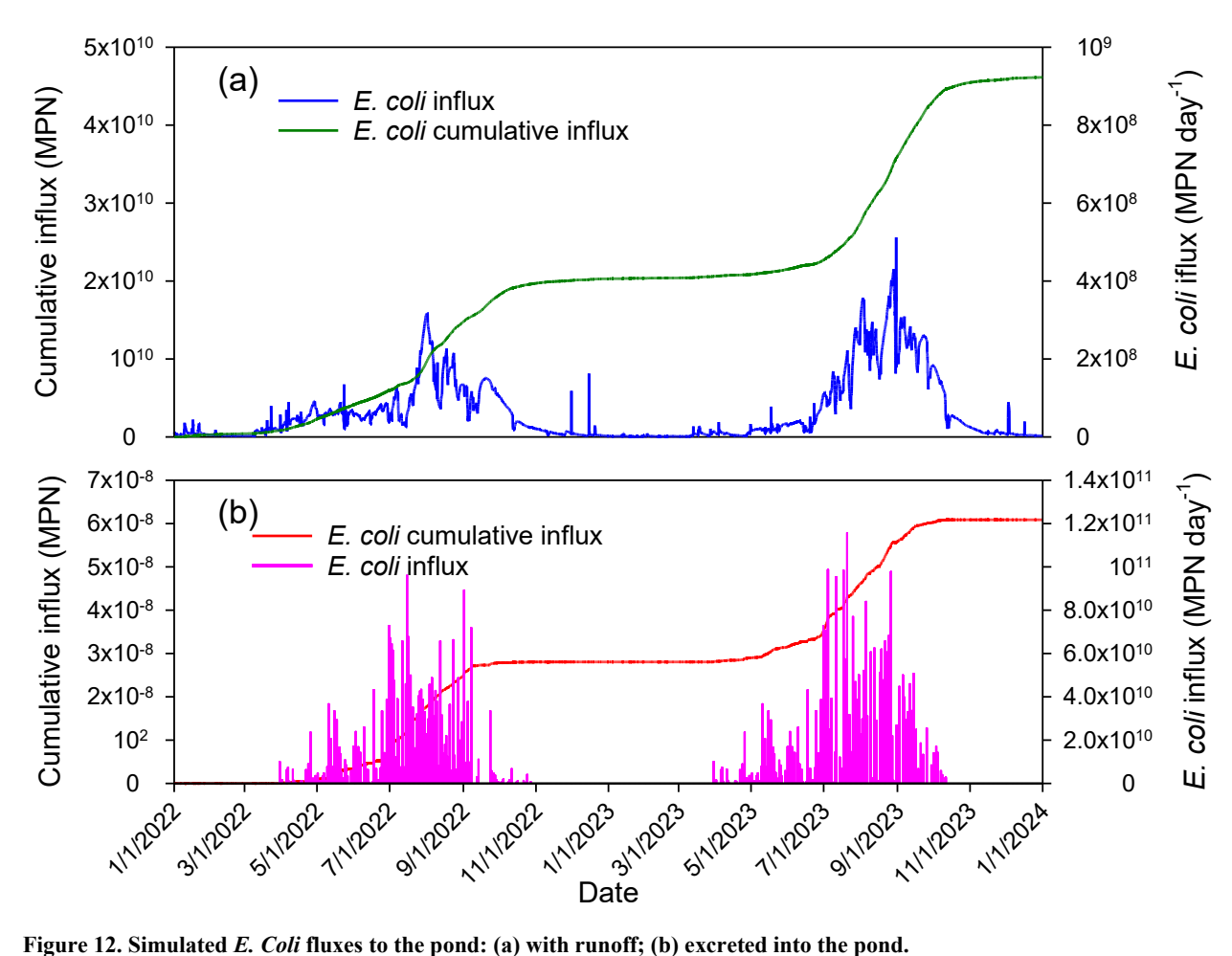


Figure 12. Simulated E. Coli fluxes to the pond: (a) with runoff; (b) excreted into the pond.





Simulated and observed concentrations of *E. Coli* were each averaged over the interior and nearshore sampling locations (Figure 13). Averaged values of concentrations at the nearshore locations (17-26) were approximately three times higher than the average of concentrations sampled at interior locations (1-15). Elevated nearshore concentrations may be explained by flushing bacteria to the pond during runoff and direct excretion by bathing cattle, which, according to monitoring, spent most of their time grouped close to the shore.

The summary data in Figure 13 show that the model describes seasonal average concentration patterns relatively well. However, observed concentrations significantly declined during autumn 2022 and 2023 compared to the model simulation. Clear, shallow water can cause deeper penetration of solar radiation. De Brauwere et al. (2014) indicate that the inactivation of bacteria is caused by UV irradiation. To account for the latter, some models add a term to the overall decay parameter due to sunlight (McCorquodale et al., 2004) or use a decay term depending on the intensity of the solar radiation (Kashefipour et al., 2006). The decrease in the nutrients in water in the fall can also be the reason for the reduction of *E. coli* concentration.

The descriptive statistics of measured and simulated average concentrations were close when computed over the observation period. The minimum and maximum averages across the pond concentrations were 3.56 and 525.1 for observed and 4.08 and 479.4 MPN (100 mL) for simulated data, respectively. The mean logarithms of average concentrations were 1.70+-0.47 and 1.99+-0.67 for the measured and simulated data, respectively. The correlation coefficient between measured and simulated logarithms of average concentrations was 0.483. This value was significant at a 0.01 significance level and indicated a moderate correlation.



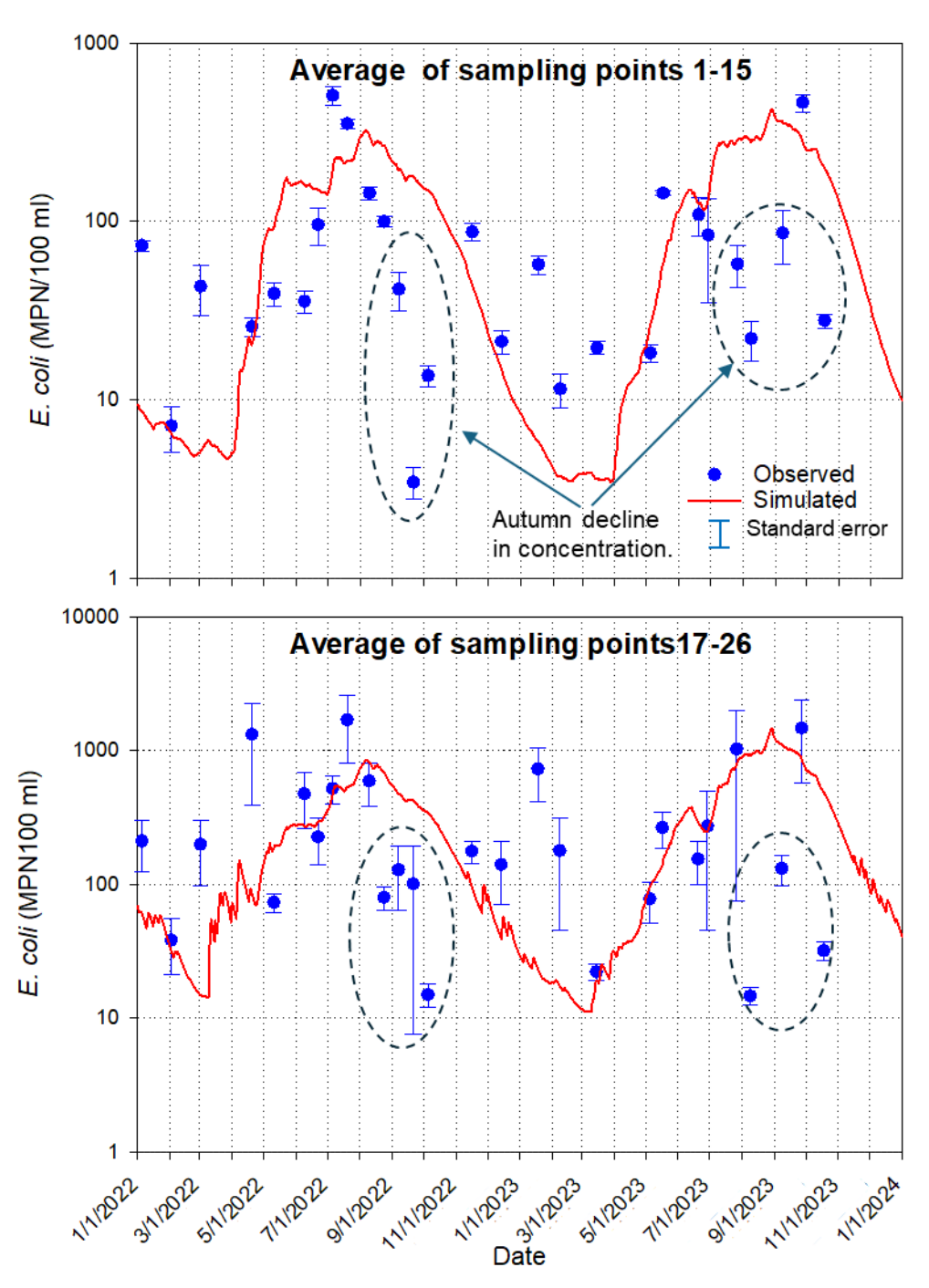


Figure 13. Average *E. coli* concentrations in the pond's interior (1-15) and nearshore (17-26) sampling locations. Dashed circles indicate an autumn decline in concentrations.





4. Discussion

Applying mechanistic fate and transport models relies on model parameter values typically obtained via model calibration. Several factors make the site-specific calibration of microbial fate and transport parameters difficult and sometimes unfeasible. The spatiotemporal variability of microbial concentrations in ponds is very high (Havelaar et al., 2017; Stocker et al., 2021), indicating the need to collect large numbers of samples. The collection and analysis of those samples appear to be unfeasible. That precludes establishing a proper monitoring program for efficient model calibration. The high spatiotemporal variability emphasized the scale mismatch between the water sample size and the water volume, and this sample is used to characterize a much larger water volume used for mass balance computation in the hydrological models.

Flow sub-model parameters have satisfactorily estimated more easily obtainable properties, such as clay or sand content and bulk density (Schaap et al., 2001). Analogous predictive relationships have not been developed, partially because the potential predictors of microorganism survival or release rate have been shown to be dependent on environmental variables that were themselves variable in space and time.

Compendia of microorganism release and survival parameters (Park et al., 2016) show that the parameter values encompass wide numerical ranges and that it is challenging to attribute fate and transport parameter values to specific environmental conditions or management practices. These factors so far substantially limit the applicability of microbial fate and transport modeling. On the other hand, such modeling is in demand due to the need for projections of microbial water quality changes due to environmental changes, adaptation practices, site-specific trade-offs between different water quality aspects, multiple ownership and management along or around irrigation water sources, etc.

In this situation, a relatively important question is: What accuracy can be expected in fate and transport predictions made with average or typical fate and transport parameter values? In other words, given the high spatial variability of microbial concentrations, how significant are the differences between observed and simulated concentrations with average parameter concentrations? The answers to those questions are surprisingly scarce, as the published modeling reports focus on calibration results. These questions have not been researched for agricultural ponds. Results of this work show that if the animal behavior patterns are known, the seasonal trends and magnitudes of pond water microbial pollution can be estimated. Quantifying such patterns for cattle ponds has not been done so far. However, it presents a promising avenue for research.

We realize that the system parameters we have studied are subject to multiple sources of uncertainty. Quantifying this uncertainty and running ensemble simulations with parameters treated as random values presents an interesting avenue for future research. Results of this work, obtained with mean parameter values from various sources, indicate that determining the statistical properties of the bacteria sources can be a first feasible step in that direction.





415 **5.** Conclusions

427

416 This study developed the first mechanistic numerical model for bacteria transport from grazing land around a cattle pond. The 417 model was based on the HGS software, simulating fully coupled surface-subsurface flow and transport. The model was tested to simulate E. coli fate and transport in a small pastureland watershed in Georgia, USA, using observations from 2021-2023. 418 419 The primary goal was to simulate the temporal and spatial distribution of E. coli concentration in the pond. All parameters for 420 this simulation were taken from the literature or estimated from published data. The exception was the rate of E. coli input to 421 the pond from the direct depositions from animals, since such data were not found in the literature. The non-calibrated model 422 could mimic E. coli temporal concentration patterns and peak times reasonably well in most of the pond's sampling locations. There were seasonal differences in correspondence between simulated and measured E. coli time series, and the magnitude of 423 concentration peaks was poorly predicted in some sampling locations. Predictions of the average across-pond concentrations 424 425 were expected to be moderately accurate. Quantification of microbial inputs for cattle ponds has not been done so far. Still, it 426 presents a promising avenue to estimate the microbial water quality in cow ponds using the data accumulated in past research.

CRediT authorship contribution statement

- 428 Alexandr Yakirevich: methodology, investigation, formal analysis, software, writing original draft; Alisa Coffin: supervision,
- 429 methodology, investigation, data acquisition, resources, formal analysis, writing review and editing; Andrew Widmer: data
- 430 acquisition, resources; Oliva Pisani: resources, writing review and editing, Robert Hill: supervision, software; Yakov
- 431 Pachepsky: conceptualization. Project administration, funding acquisition

432 Declaration of competing interest

- 433 The authors declare that they have no known competing financial interests or personal relationships that could have appeared
- 434 to influence the work reported in this paper.

435 Acknowledgements

- 436 This research was supported by the USDA-ARS projects (6048-13000-028-000D "Shifting the Balance of Water Resources
- 437 and Interacting Agroecosystem Services toward Sustainable Outcomes in Watersheds of the Southern Coastal Plain," non-
- 438 assistance cooperative agreements 58-8042-3-030 "Modeling Fate and Transport of Indicator and Pathogenic Organisms to
- 439 Assess Microbial Water Quality of Irrigation Water Sources, "and 58-8042-0-064 "Monitoring and Modeling Microbial
- 440 Quality of Irrigation Water"





441 Data availability

- 442 Data will be made available on request.
- 443444

448

452

454

459

461

466

- 445 Appendix A: Equations to calculate E. coli concentration released from cowpats at the soil surface (3rd-kind boundary
- 446 condition concentration).
- 447 For day t, the content of microorganism in the applied manure is calculated by (Franz et al., 2008; Martinez et al., 2013):
- 449 $m_i(t) = m_i(t-1)e^{-k_{s,m}}$ (A1)
- 451
- Where $k_{s,m}$ is the rate coefficient which is the function of temperature T at time t, (d⁻¹)
- 453 $k_{s,m} = \begin{cases} k_{s,m,1}, & t \le t_{s,m,1} \\ k_{s,m,2}(T), & t > t_{s,m,1} \end{cases}$ (A2)
- 455 $t_{s,m,1}$ is the duration of the first stage, d, T is the average daily temperature, °C, and $k_{s,m,1}$ and $k_{s,m,2}(T)$ the survival rates at the
- 456 first and second survival stages are respectively.
- 457 The bacterial population may grow, remain stable, or die off during the first survival stage, and decrease during the second
- 458 stage of survival. On the second stage, the values of $k_{s,m,2}(T)$ can be described with the Q10 model (Martinez et al., 2013).
- 460 $k_{s,m,2}(T) = k_{s,m,2}(20)Q_{10,m}^{\frac{T-20}{10}}$ (A3)
- where $k_{s,m,2}(20)$ is the survival rate at 20 °C, $Q_{10,m}$ reflects the sensitivity of $k_{s,m,2}$ to a temperature that is equal to the change
- in survival rate occurring as temperature changes by 10 °C.
- 464 The concentration of released microorganism C_m is calculated according to Bradford and Schijven (2002) as
- 465 $C_{man}(t) = \frac{dM_{man}}{Rdt} = \frac{M_0 \alpha_m}{R} (1 + \alpha_m \beta_m t)^{-(1+1/\beta_m)}$ (A4)
- $C_m(t) = m_i E_r C_{man}(t) \tag{A5}$
- Where M_{man} is the cumulative cowpat mass released into the aqueous phase (g), R is rain intensity, cm/h, $\alpha_{\rm m}$ (h⁻¹) and $\beta_{\rm m}$ are
- 470 fitting parameters defining the shape of the release curve, and M_0 is the initial mass of cowpats (g/cm²), C_{man} is the aqueous





- 471 manure concentration (g cm⁻³), m_i is content of microorganism in the cowpats (CFU g⁻¹), E_r is microorganism release
- 472 efficiency.





474 References

- 475 Balkcom, G., Touchstone, T., Kammermeyer, K., Vansant, V., Martin, C., Van Brackle, M., Steele, G., & Bowers, J. Waterfowl
- management in Georgia. Georgia Department of Natural rresources. Available at https://geotgiawildlife.com. Last
- 477 assessed on 2/20/2025.
- Benham, B.L., Baffaut, C., Zeckoski, R.W., Mankin, K.R., Pachepsky, Y.A., Sadeghi, A.M., Brannan, K.M., Soupir, M.L., Habersack, M.J., 2006. Modeling bacteria fate and transport in watershed models to support TMDLs. Trans. ASABE 49 (4), 987–1002.
- Blaustein, R. A., Pachepsky, Y., Hill, R. L., Shelton, D. R., & Whelan, G. (2013). Escherichia coli survival in waters: temperature dependence. *Water research*, 47(2), 569-578.
- Blaustein, R.A., Pachepsky, Y., Hill, R.L., Shelton, D.R. and Whelan, G., 2013. Escherichia coli survival in waters: temperature dependence.

 Water research, 47(2), pp.569-578.
- Blume, L.J., Perkins, H.F. and Hubbard, R.K., 1987. Subsurface water movement in an upland coastal plain soil as influenced by plinthite.

 Soil Science Society of America Journal, 51(3), pp.774-779.
- Bosch, D. D., Sheridan, J. M., Lowrance, R. R., Hubbard, R. K., Strickland, T. C., Feyereisen, G. W., & Sullivan, D. G. (2007). Little river experimental watershed database. *Water Resources Research*, *43*(9).
- Bradford, S.A., and J. Schijven. 2002. Release of Cryptosporidium and Giardia from dairy calf manure: Impact of solution salinity. Environ.

 Sci. Technol. 36:3916–3923.
- 490 Bradford, S.A., Morales, V.L., Zhang, W., Harvey, R.W., Packman, A.I., Mohanram, A., and Welty, C. 2013. Transport and fate of microbial pathogens in agricultural settings. Critical Reviews in Environmental Science and Technology 43, 775–893.
- 492 Cho, K.H., Pachepsky, Y.A., Kim, M., Pyo, J.C., Park, M.H., Kim, Y.M., Kim, J.W., Kim, J.H., 2016. Modeling seasonal variability of fecal coliform in natural surface waters using the modified SWAT. J. Hydrol. 535, 377–385.
- Cho, K., Wolny, J., Kase, J. A., Unno, T., & Pachepsky, Y. (2021). Interactions of E. coli with algae and aquatic vegetation in natural waters. Water research, 117952.
- 496 Collins, R., Rutherford, K., 2004. Modelling bacterial water quality in streams draining pastoral land. Water Res. 38 (3), 700–712.
- 497 Currle, F., Therrien, R. and Schilling, O.S., 2024. Explicit simulation of reactive microbial transport with a dual-permeability, two-site
- kinetic deposition formulation using the integrated surface-subsurface hydrological model HydroGeoSphere (rev. 2699).

 EGUsphere, 2024, pp.1-26.
- Danielescu, S. (2022). Development and Application of ETCalc, a Unique Online Tool for Estimation of Daily Evapotranspiration.

 Atmosphere-Ocean, 61(3), 135–147. https://doi.org/10.1080/07055900.2022.2154191.
- Daniels, R.B., Perkins, H.F., Hajek, B.F. and Gamble, E.E., 1978. Morphology of discontinuous phase plinthite and criteria for its field identification in the Southeastern United States. Soil Science Society of America Journal, 42(6), pp.944-949.
- David, M. M., and Haggard, B. E. 2011. Development of regression-based models to predict fecal bacteria numbers at select sites within the Illinois River watershed, Arkansas and Oklahoma, USA. Water, Air, and Soil Pollution 215, 525–547.
- 506 de Brauwere, A., Ouattara, N. K., & Servais, P. (2014). Modeling Fecal Indicator Bacteria Concentrations in Natural Surface Waters: A

Environmental

508 https://doi.org/10.1080/10643389.2013.829978.

Critical

Reviews

Review.

507

Ferguson, C., Husman, A.M. d. R., Altavilla, N., Deere, D., and Ashbolt, N. 2003. Fate and transport of surface water pathogens in watersheds. Critical Reviews in Environmental Science and Technology 33, 299–361.

Science

and

Technology,

44(21),

2380-2453.





- 511 Franz, E., Semenov, A.V., Termorshuizen, A.J., De Vos, O.J., Bokhorst, J.G., Van Bruggen, A.H.,
- Havelaar, A. H., Vazquez, K. M., Topalcengiz, Z., Muñoz-Carpena, R., & Danyluk, M. D. (2017). Evaluating the US food safety
- 513 modernization act produce safety rule standard for microbial quality of agricultural water for growing produce. Journal
- 514 of food protection, 80(11), 1832-1841
- 515 in 36 Dutch soils. Environ. Microbiol. 10 (2), 313–327.
- 516 Iqbal, M. S., & Hofstra, N. (2019). Modeling Escherichia coli fate and transport in the Kabul River Basin using SWAT. *Human*
- 517 and Ecological Risk Assessment: An International Journal, 25(5), 1279-1297.
- 518 Kondo T, Sakai N, Yazawa T, Shimizu Y.Sci Total Environ. 2021 June 20;774:145075. doi: 10.1016/j.scitotenv.2021.145075. Epub
- 519 2021 February 3.PMID: 33609845
- 520 Moriarty, E. M., Karki, N., Mackenzie, M., Sinton, L. W., Wood, D. R., & Gilpin, B. J. (2011). Faecal indicators and pathogens in
- selected New Zealand waterfowl. New Zealand Journal of Marine and Freshwater Research, 45(4), 679-688.
- 522 Oliver, D. M. (2014). Seasonal and within-herd variability of E. coli concentrations in fresh dairy faeces. Letters in applied
- 523 *microbiology*, 59(1), 86-92.
- 524 Park, Y., Pachepsky, Y., Shelton, D., Jeong, J., & Whelan, G. (2016). Survival of manure-borne Escherichia coli and fecal
- 525 coliforms in soil: temperature dependence as affected by site-specific factors. *Journal of Environmental Quality*, 45(3),
- 526 949-957.
- 527 Schaap, M. G., Leij, F. J., & Van Genuchten, M. T. (2001). Rosetta: A computer program for estimating soil hydraulic parameters
- 528 with hierarchical pedotransfer functions. *Journal of hydrology*, 251(3-4), 163-176.
- 529 Sowah, R. A., Bradshaw, K., Snyder, B., Spidle, D., & Molina, M. (2020). Evaluation of the soil and water assessment tool
- 530 (SWAT) for simulating E. coli concentrations at the watershed-scale. Science of the Total Environment, 746, 140669.
- Ferguson, C. M., Coote, B. G., Ashbolt, N. J., and Stevenson, I. M. 1996. Relationships between indicators, pathogens and
- water quality in an estuarine system. Water Research 30, 2045–2054.

533 Gao, G., Falconer, R.A. and Lin, B., 2015. Modelling the fate and transport of faecal bacteria in estuarine and coastal waters. Marine pollution

- 534 bulletin, 100(1), pp.162-168.
- 535 Gautam, B., Kasi, M., Lin, W., 2006. Determination of fecal coliform loading and its impact
- on river water quality for TMDL development. WEF Proc. 2006 (9), 3851–3874.
- Hansen, S., Messer, T., Mittelstet, A., Berry, E.D., Bartelt-Hunt, S. and Abimbola, O., 2020. Escherichia coli concentrations in waters of a
- reservoir system impacted by cattle and migratory waterfowl. Science of The Total Environment, 705, p.135607.
- Henderson, S.M., Nielson, J.R., Mayne, S.R., Goldberg, C.S. and Manning, J.A., 2024. Transport and mixing observed in a pond: Description
- of wind-forced transport processes and quantification of mixing rates. Limnology and Oceanography, 69(9), 2180-2192.
- Hong, S.M., Morgan, B.J., Stocker, M.D., Smith, J.E., Kim, M.S., Cho, K.H. and Pachepsky, Y.A., 2024. Using machine learning models
- 542 to estimate Escherichia coli concentration in an irrigation pond from water quality and drone-based RGB imagery data. Water
- 543 Research, p121861.
- Hong, E.M., Park, Y., Muirhead, R., Jeong, J. and Pachepsky, Y.A., 2018. Development and evaluation of the bacterial fate and transport
- module for the Agricultural Policy/Environmental eXtender (APEX) model. Science of the Total Environment, 615, pp.47-58.
- 546 Joe, J., Rick, N., Snouwaert, E., 2009. Hangman (Latah) Creek Watershed Fecal Coliform,
- 547 Temperature, and Turbidity Total Maximum Daily Load, Water Quality Improvement





- Report. Washington State Department of Ecology, Washington D.C. (Publication no.
- 549 09-10-030a).
- 550 Kashefipour, S. M., Lin, B., and Falconer, R. A. 2002. Dynamic modelling of bacterial concentrations in coastal waters: Effects of solar
- radiation on decay. In J. J. Guo, et al. (Eds.), Advances in hydraulics and water engineering, Vols. 1 and 2: Proceedings, World
- Scientific: Singapore, pp. 993–998.
- Kuang, W., Huang, Q. and Xiao, G., 2024. Modeling Escherichia coli concentrations for health risk analysis in the Three Gorges Reservoir
- Region, Chongqing, China. Journal of Hydrology, p.131511.
- Li, L., J. Qiao, G. Yu, L. Wang, H.-Y. Li, C. Liao, and Z. Zhu. 2022. "Interpretable Tree-Based Ensemble Model for Predicting Beach Water
- 556 Quality." Water Research 211:118078. https://doi.org/10.1016/j.watres.2022.118078.
- Mankin, K.R., Wang, L., Hutchinson, S.L. and Marchin, G.L., 2007. Escherichia coli sorption to sand and silt loam soil. Transactions of the
- 558 ASABE, 50(4), 1159-1165.
- Martinez, G., Pachepsky, Y. A., Shelton, D. R., Whelan, G., Zepp, R., Molina, M., & Panhorst, K. 2013. Using the Q10 model to simulate
- *E. coli* survival in cowpats on grazing lands. Environment International, 54, 1-10.
- 561 McCorquodale, J. A., Georgiou, I., Carnelos, S., and Englande, A. J. 2004. Modeling coliforms in storm water plumes. Journal of
- Environmental Engineering and Science 3, 419–431.
- Nennich, T.D., Harrison, J.H., Vanwieringen, L.M., Meyer, D., Heinrichs, A.J., Weiss, W.P., St-Pierre, N.R., Kincaid, R.L., Davidson, D.L.
- and Block, E., 2005. Prediction of manure and nutrient excretion from dairy cattle. Journal of Dairy Science, 88(10), 3721-3733.
- Nueman S.P. 1990. Universal scaling of hydraulic conductivities and dispersivities in geologic media. Water Resources Research, 26 (8),
- 566 1749-1758.
- Park, Y., Pachepsky, Y., Shelton, D., Jeong, J. and Whelan, G., 2016. Survival of manure-borne *Escherichia coli* and fecal coliforms in soil:
- temperature dependence as affected by site-specific factors. Journal of Environmental Quality, 45(3), 949-957.
- Renwick WH, Oh O. 2006. Small artificial ponds in the United States: impacts on sedimentation and carbon budget, p 738–744. Proceedings
- 570 of the 8th Federal Interagency Sedimentation Conference. Advisory Committee on Water Information, US Geological Survey, US
- 571 Department of the Interior, Reston, VA https://water.usgs.gov/osw/ressed/references/Renwick-2006-8thFISC.pdf
- 572 Sadeghi, A.M., Arnold, J.G., 2002. A SWAT/microbial submodel for predicting pathogen loadings in surface and groundwater at watershed
- and basin scales. Total Maximum Daily Load (TMDL) Environmental Regulations. ASAE Publication 701P0102. ASAE, St.
- 574 Joseph, Mich, pp. 56–63.
- 575 Stocker, M.D., Pachepsky, Y.A. and Hill, R.L., 2022. Prediction of E. coli concentrations in agricultural pond waters: application and
- 576 comparison of machine learning algorithms. Frontiers in Artificial Intelligence, 4, p.768650.
- 577 Stocker, M., Yakirevich, A., Guber, A., Martinez, G., Blaustein, R., Whelan, G., Goodrich, D., Shelton, D. and Pachepsky, Y., 2018.
- Functional evaluation of three manure-borne indicator bacteria release models with multi-year field experiment data. Water, Air,
- 579 & Soil Pollution, 229, pp.1-18.
- 580 Therrien, R., Sudicky, E. A., & McLaren, R. G. (2010). HydroGeoSphere: A Three-Dimensional Numerical Model Describing Fully-
- 581 Integrated Sub-Surface and Surface Flow and Solute Transport. Groundwater Simulations Group, 1-369.
- van der Meulen, E. S., Tertienko, A., Blauw, A. N., Sutton, N. B., van de Ven, F. H. M., Rijnaarts, H. H. M., & van Oel, P. R. (2024). A
- review of prediction models for E. coli in urban surface waters. Urban Water Journal, 21(5), 539-548.
- 584 https://doi.org/10.1080/1573062X.2024.2313634





- Van Genuchten, M.T., 1980. A closed-form equation for predicting the hydraulic conductivity of unsaturated soils. Soil science society of America journal, 44(5), pp.892-898.
- Vazquez KM, Muñoz-Carpena R, Danyluk MD, Havelaar AH. 2021. Parsimonious mechanistic modeling of bacterial runoff into irrigation ponds to inform food safety management of agricultural water quality. Appl Environ Microbiol 87: e00596-21. https://doi.org/10.1128/AEM.00596-21.
- Watson, T.W. The geohydgology of Ben Hill, Irwin, Tift, Turner and Worth counties, Georgia. Hydrologic Atlas 2, Atlanta, 1976.
- Wolska, L., Kowalewski, M., Potrykus, M., Redko, V. and Rybak, B., 2022. Difficulties in the modeling of *E. coli* spreading from various sources in a coastal marine area. Molecules, 27(14), p.4353.
- Yao, F., Band, L. E., Cheng, F. Y., Rosentreter, J., Yang, K., & Wang, C. (2024). A new high-resolution global lake area dataset for constraining biogeochemical fluxes from inland water bodies. AGU Fall Meeting Abstracts, 2024(1177), H53H-1177.